

Light Curve Analysis of Ground-Based Data from Exoplanets Transit Database

**F. Davoudi^{1,2}; S. J. Jafarzadeh^{1,2}; A. Poro^{1,2}; O. Basturk³; S. Mesforoush²; A. Fasihi Harandi²;
MJ. Gozarandi^{1,2}; Z. Zare Mehrjardi^{1,2}; P. D. Maley⁴; S. Khakpash^{2,5}; K. Rokni²; A. Sarostad²**

¹ The International Occultation Timing Association-Middle East Section, info@iota-me.com

² The Six Summer School of Astronomy (IOTA/ME), Khayyam Observatory, Mahdasht, Iran

³ Ankara University, Faculty of Science, Astronomy and Space Sciences Department, TR-06100, Tandogan, Ankara, Turkey

⁴ The International Occultation Timing Association, Carefree AZ, USA

⁵ Department of Physics, Lehigh University, 16 Memorial Drive East, Bethlehem, PA 18015, USA

Abstract

Photometric observations of exoplanet transits can be used to derive the orbital and physical parameters of an exoplanet. We analyzed several transit light curves of exoplanets that are suitable for ground-based observations whose complete information is available on the Exoplanet Transit Database (ETD). We analyzed transit data of planets including HAT-P-8 b, HAT-P-16 b, HAT-P-21 b, HAT-P-22 b, HAT-P-28 b and HAT-P-30 b using the AstromageJ (AIJ) software package. In this paper, we investigated 82 transit light curves from ETD, deriving their physical parameters as well as computing their mid-transit times for future Transit Timing Variation (TTV) analyses. The Precise values of the parameters show that using AIJ as a fitting tool for follow-up observations can lead to results comparable to the values at the NASA Exoplanet Archive (the NEA). Such information will be invaluable considering the numbers of future discoveries from ground and space-based exoplanet surveys.

Keywords: Exoplanet, Transit, Photometry, AIJ, ETD

Introduction

Ground-based observations alongside space missions have great scientific potential in the discovery of new exoplanets and validating their parameters. Various physical parameters can be deduced using transit light curves. Of course, the number and accuracy of these parameters depend on the accuracy of the photometry, the type of exoplanet system, and the initial assumptions of the orbit using Kepler's laws. Ground-based exoplanet surveys have made a lot of contributions to this field. In this paper, we chose cases derived from Hungarian-made Automated Telescope (HAT) surveys.

The Hungarian-made Automated Telescope Network (HATNet) has been in operation since 2003, with the key science goal being the discovery and accurate characterization of Transiting Extrasolar Planets (TEPs) around bright stars in the Northern hemisphere (Bakos et al. 2004). HATNet consists of six wide field automated telescopes: four of these are located at the Fred Lawrence Whipple Observatory (FLWO) in Arizona and two on the roof of the Submillimeter Array hangar of the Smithsonian Astrophysical Observatory (SAO) in Hawaii. Furthermore, the HATSouth network was the first global network of telescopes using identical instrumentation. They have been important contributors to the rapidly developing field of exoplanets, motivating and influencing observational techniques, theoretical studies, and also actively shaping future instrumentation for the detection and characterization of exoplanets (Bakos, 2018).

Throughout this article, we improved the parameters of the planets in proportion to the Exoplanet Transit Database (ETD)¹. We analyzed several transit curves of exoplanets based on data from ETD. ETD is a project of the Variable Star and Exoplanet Section of the Czech Astronomical Society. It is created to supply observers with such useful information as transit predictions, Transit Timing Variation (TTV); in addition, it enables the user to plot light curves depicting their depth and duration. The main goal of the ETD is to gather all available light curves from professional and also amateur astronomers. They use a simple analytical model of the transit to calculate the central time of transit, its duration and the depth of the transit. These values are then plotted into the observed computed diagrams (O-C) that represent the last part of the application (Poddan'y et al. 2009). In the Data section below, we discuss how to select data from the ETD and specifications of the observations.

In the Method section below, we describe the factors that show the distinction between AIJ and ETD discussing how to use the AIJ package efficiently. AIJ is a graphical software package for general image processing. It simplifies light curve plotting, especially for applications requiring ultra-precise light curves such as exoplanet transits (Mandel & Agol, 2002). AIJ is a Java program and its astronomical algorithms are based on codes from JSkyCal; this package is compatible with all operating systems (Collins et al. 2017). Transit parameters are calculated from the best fit model by AIJ including the planetary radius in units of the stellar radius, R_p / R_* , the orbital inclination i , the transit duration t_{14} and the mid-transit time t_c . In the Data Analysis section, we summarize the calculated values of the parameters of each exoplanet using AIJ and determine uncertainties in the parameters of transit with a differential evolution Markov Chain Monte Carlo (MCMC) simulation. Finally, in the Results section, we compared values of the output parameters of planets with that from the NASA Exoplanet Archive (the NEA) database².

The NEA is operated by the California Institute of Technology under contract with the National Aeronautics and Space Administration's Exoplanet Exploration Program. This archive combines a database of the confirmed exoplanets and host star properties with key public data sets from space and ground-based surveys; it also provides quantitative analysis tools to work with this data. Examples of the data included are stellar parameters (positions, magnitudes, and temperatures), exoplanet parameters (masses and orbital parameters), and discovery/characterization data (published radial velocity curves, photometric light curves, images, and spectra). The contents of each data set are fully described as part of the archive documentation. The Exoplanet Archive also includes over 2.9 million light curves, including public data from space missions and several ground-based surveys (Akesoni et al. 2013).

So, it is possible to derive valuable information by analyzing transit light curves of exoplanets, provided by even amateur astronomers with access to relatively modern observing equipment, by using off-the-shelf analysis software as AIJ and web services such as EXOFAST. The mid-transit times as the results of our work will constitute a processed input to perform a Transit Timing Variation (TTV) analysis for these exoplanets.

Data Sets

Exoplanets that we have studied in this paper are HAT-P-8 b (D.W. Latham et al. 2009), HAT-P-16 b (L.A. Buchhave et al. 2010), HAT-P-21 b (G.Á. Bakos et al. 2011), HAT-P-22 b (G.Á. Bakos et al. 2011), HAT-P-28 b (L.A. Buchhave et al. 2011), and HAT-P-30 b (J.A. Johnson et al. 2011) whose light curves are taken from the ETD. We chose these planets because the number of light curves of their transits is appropriate and their observations have been made in the last ten years. They have suitable brightnesses to enable ground-based observations (maximum magnitude 15). In addition to the suitability of data quality, we made a selection by eye. For example, we chose those for analysis that have sufficiently out-of-transit data points and show a clear decrease of the brightness in the light curve during a transit. The orbital period of each exoplanet is less than 5 days. Duration of transits is less than 0.2 day and these planets only orbit around one star.

Data are provided by different observers from different geographical locations. For example, for HAT-P-8 b 14 light curves were examined for which their observational information is listed in Table.2. The first column refers to the

¹ <http://var2.astro.cz/ETD/>

² <https://exoplanetarchive.ipac.caltech.edu/>

data file number, the next five columns refer to the observer's name, observation dates, the filter type, optical size, and the CCD model used, respectively. The last column refers to the data quality of individual light curves which is indicated by a number from 1 (for the best) to 5 (for the worst) based on the records in the ETD that are divided into five groups according to their data quality index DQ. While computing the DQ index of the light curve, the following relation is used

$$\alpha = \frac{\delta}{S} \sqrt{\rho} \quad (1)$$

Here α is a temporary data quality index, S is the mean absolute deviation of the data from their fit and $\rho = N/l$ is the data sampling, where l is the length of observing run in minutes. The number α is further transformed for better lucidity to the scale from 1 to 5 where 1 presents the best quality data and the value 5 the worst data (Table 1). They provide only the results of mid-transit time, transit depth and length of the transit, not the whole light curve (Poddan'y et al. 2009).

Table 1. The distribution of the quality of the light curves according to their DQ index

DQ index	1	2	3	4	5
Threshold	$\alpha \geq 9.5$	$9.5 > \alpha \geq 6.0$	$6.0 > \alpha \geq 2.5$	$2.5 > \alpha \geq 1.3$	$1.3 > \alpha$

In the following tables data for the six exoplanets light curve information are shown. Tables 2-7 illustrate initial data information for HAT-P-8 b, HAT-P-16 b, HAT-P-21 b, HAT-P-22 b, HAT-P-28 b and HAT-P-30 b respectively.

Table 2. Initial data information for HAT-P-8 b

NO.	Observer	Observation Date	Filter	Optic size (mm)	CCD Model	DQ
1	H. Kučáková	2009-07-22	R	200	ST-8XME	3
2	B. Norby	2009-08-03	R	254	- ³	3
3	A. Ayiomamitis	2009-08-27	Clear	162.56	ST-10XME	3
4	G. Srdoc	2009-08-27	R	304.8	-	3
5	H. Kučáková	2009-08-29	R	200	ST8-XME	3
6	J. Trnka	2009-08-29	Clear	200	ST-9E	3
7	G. Srdoc	2009-08-30	R	304.8	-	3
8	F. Hormuth	2010-09-02	R	1230	DLR-MKIII	1
9	N. Ruocco	2010-09-02	R	304.8	ST-7	3
10	G. Marino	2010-09-02	Clear	317.5	QSI 516wsg	3
11	K. Hose	2011-03-17	R	200	ST-8	3
12	R. Uhlár	2011-08-30	R	304.8	ST9-XE	5
13	K. Hose	2012-09-23	R	200	-	2
14	R. Naves	2016-08-27	R	304.8	ST10XME	2

Table 3. Initial data information for HAT-P-16 b

NO.	Observer	Observation Date	Filter	Optic size (mm)	CCD Model	DQ
1	M. Vrašťák	2010-09-30	Clear	240	G2	2
2	J. Világi et al.	2010-11-10	Clear	600	-	2
3	S. Shadick	2010-11-01	Clear	304.8	STL1301	3
4	S. Shadick	2011-10-17	Clear	304.8	ST10XME	2
5	J. Trnka	2011-10-01	Clear	200	ST-9E	3
6	T. Sauer	2011-10-06	R	203.2	ST-10	3
7	S. Shadick	2011-10-17	I	304.8	STL1301	3

³ When the information about the CCD is not available, it is represented by a dash.

8	R. Garcia	2012-01-10	V	355.6	-	3
9	J. Mravik et al.	2012-10-23	Clear	203.2	ST-7	3
10	F.G. Horta	2013-09-12	V	305	FLI PL1001E-1	3
11	P. Benni	2013-11-06	Clear	203.2	ST8300M	3
12	A. Ayiomamitis	2013-11-18	Clear	305	ST-10XME	3
13	F. Scaggiante et al.	2014-01-06	R	410	KAF402ME	3
14	D.Molina	2015-11-09	Clear	2000	ST-8XME	2
15	F. Campos	2015-11-23	R	200	ST-8XME	3
16	D. Molina	2016-12-27	Clear	203	ST-8XME	2

Table 4. Initial data information for HAT-P-21 b

NO.	Observer	Observation Date	Filter	Optic size (mm)	CCD Model	DQ
1	R. Dreven	2011-03-09	R	200	G1 300	3
2	R. Zambelli	2011-04-14	R	254	ST-8XME	2
3	L. Trevmosa	2012-01-04	Clear	132	-	3
4	P. Benni	2014-02-14	Clear	203.2	ST8300M	3
5	J.P. Jacobsen	2016-05-19	Clear	355.6	-	3

Table 5. Initial data information for HAT-P-22 b

NO.	Observer	Observation Date	Filter	Optic size (mm)	CCD Model	DQ
1	L. Brát	2011-02-24	Clear	200	G1-0300	3
2	R. Zambelli	2011-03-14	R	254	ST-8XME	2
3	G. Marino	2012-01-26	R	200	ST-7	3
4	J.L. Haro	2013-02-11	V	250	ST-7XME	3
5	A. Ayiomamitis	2013-03-14	Clear	305	ST-10XME	2
6	V.P. Hentunen	2014-02-06	R	355.6	ST-8XME	3
7	M. Salisbury	2014-05-07	R	400	ST-10XME	2
8	CAAT group	2015-08-10	Clear	406.4	ST-7XME	3
9	R.N. Nogues	2015-08-10	R	305	ST-8XME	3
10	V.P. Hentunen	2017-01-12	R	355.6	ST-8XME	2
11	D. Molina	2018-12-11	Clear	203	ST-8XME	2

Table 6. Initial data information for HAT-P-28 b

NO.	Observer	Observation Date	Filter	Optic size (mm)	CCD Model	DQ
1	H. Kučáková	2011-09-05	Clear	304.8	ST-8XME	5
2	F. Lomoz	2011-09-05	Clear	254	G2-8300	3
3	M. Zíbar	2011-09-05	Clear	203.2	Atic 16 IC	3
4	L. Brát	2011-09-05	Clear	200	G1-0300	3
5	J. Trnka	2011-10-01	Clear	300	G1-0300	3
6	L. Brát	2011-10-01	Clear	200	G1-0300	3
7	F. Lomoz	2011-10-01	Clear	300	ST2000XM	4
8	J. Trnka	2011-10-24	Clear	200	ST-9E	3
9	S. Shadick	2011-12-27	Clear	304.8	ST-10XME	3
10	P. Benni	2013-08-09	Clear	279.4	ST-8XME	3
11	P. Benni	2013-11-21	Clear	279.4	ST-8XME	3
12	P. Benni	2014-02-06	Clear	279.4	ST-8XME	3
13	J. Gonzalez	2014-08-20	Clear	235	ST-8XME	3

14	J. Garlitz	2014-10-22	Clear	304.8	SBIG402	3
15	M. Bretton	2015-07-22	Clear	430	STL-11K	2
16	M. Bretton	2015-11-02	Clear	254	T820	2
17	M. Fleenor	2016-12-27	Clear	355	ST-10XME	2
18	C. Rude et al.	2017-01-12	R	500	SBIG6303E	3
19	M. Bretton	2018-12-11	Clear	820	FLI PL230	1
20	Y. Jongen	2018-12-29	Clear	355.6	STLX11002	3

Table 7. Initial data information for HAT-P-30 b

NO.	Observer	Observation Date	Filter	Optic size (mm)	CCD Model	DQ
1	R. Uhlář	2011-03-30	R	200	-	3
2	S. Shadick	2012-04-25	Clear	254	ST-10XME	3
3	J. Gonzalez	2012-01-26	R	235	ST-8XME	3
4	S. Shadick	2012-04-02	I	254	ST-10XME	3
5	J. Gonzalez	2012-02-21	Clear	235	ST-8XME	3
6	G. Marino	2012-02-21	R	200	ST-7	3
7	S. Shadick	2012-03-19	R	355.6	ST-10XME	3
8	R. Naves	2012-11-15	R	305	ST-8XME	3
9	S. Shadick	2013-01-18	Clear	254	ST-10XME	3
10	V. P. Hentunen	2014-02-06	Clear	355.6	ST-8XME	3
11	G. Marino	2014-02-18	I	250	ST-7	3
12	E. Sokov et al.	2014-05-07	V	500	ST-L 1001E	3
13	F. Scaggiante et al.	2015-07-22	R	410	KAF402ME	3
14	A. Christophe et al.	2015-08-10	R	600	STL6303E	3
15	D. Molina	2018-12-11	Clear	203	ST-8XME	3
16	F. Campos	2019-02-18	R	203.2	ST-8XME	2

All observations have been performed by using CCD detectors attached on small-to-medium size telescopes. The smallest telescope has a primary with the diameter 132 mm, while the largest has 2000 mm-diameter mirror. The average optics size in all observations is 323.34 mm (12.73 inches). Moreover, the majority of the telescopes were in the range of 200-400 mm (Table 8).

Table 8. The size of the optics used in the observations

Planet	The smallest optic	The largest optic	Average optics size
HAT-P-8 b	162.56 mm	1230 mm	320.57 mm
HAT-P-16 b	200 mm	2000 mm	396.41 mm
HAT-P-21 b	132 mm	355.6 mm	228.96 mm
HAT-P-22 b	200 mm	406.4 mm	294.05 mm
HAT-P-28 b	200 mm	820 mm	317.97 mm
HAT-P-30 b	200 mm	600 mm	300.90 mm

Method

Photometric datasets from ETD include differential magnitudes with respect to the mid-time of CCD exposures, in either Julian Dates (JD) or Heliocentric Julian Dates (HJD). Because of the high accuracy of Barycentric Julian Dates (BJD) in comparison to other reference frames, the HJD was formally deprecated by the International Astronomical

Union (IAU) in 1991 in favor of the BJD, a time referenced to the Solar System Barycenter (SSB) (Eastman et al. 2010). Therefore we converted our times from JD_UTC or HJD_UTC to BJD_TDB through the web service⁴.

For each exoplanet, we processed its data with the AIJ. A transiting exoplanet is modeled as an eclipse of a spherical star by an opaque planetary sphere. The model is characterized by six physical values, plus a baseline flux level, F_0 . The six physical parameters are the planetary radius in units of the stellar radius, R_p / R_* , the distance between the planet and star scaled in units of the stellar radius, a / R_* , the transit centre time, T_C , the impact parameter of the transit, b , and the quadratic limb darkening parameters, u_1 and u_2 . The orbital inclination can be calculated from the model parameters as

$$i = \cos^{-1} \left(b \frac{R_*}{a} \right). \quad (2)$$

The best fit model is found by minimizing χ^2 of the model residuals using the downhill simplex method to find the local minima. Light curve detrending is accomplished by including a χ^2 contribution for each selected detrend parameter in the overall light curve fit. The χ^2 contribution for all n detrend parameters are calculated at each step of the fitting process as

$$\chi_D^2 = \sum_{k=1}^m \frac{(o_k - (\sum_{j=1}^n c_j D_{jk}) - E_k)^2}{\sigma_k^2} \quad (3)$$

here j indexes the detrend parameters, k indexes the samples of the light curve, m is the total number of samples in the light curve, o_k is the observed normalized differential target flux, c_j is the fitted linear coefficient for the detrend parameter values D_{jk} , E_k is the expected value of the flux (which is the normalized transit model value corresponding to the time of the k_{th} data sample), and σ_k is the error in the normalized differential target flux for each sample.

Furthermore, the best linear fit of a trend dataset (airmass in this case) to the light curve is found by using AIJ. It is possible to see how the fit is improved by detrending for the airmass. A good guide for whether a detrending parameter is effective is to view the Bayesian Information Criterion (BIC) value (P.M. Bentler 1995). If it reduces by more than 2.0, then airmass should be detrended. In other words, the fit with the lowest BIC value indicates the preferred model. The BIC is calculated as

$$BIC = \chi^2 + p \ln n \quad (4)$$

Where p is the number of fitted parameters, and n is the number of fitted data points. The χ^2 contribution represents the goodness of the linear fit of the detrend parameter to the light curve after subtracting the light curve model corresponding to the current fit step (Collins et al. 2017).

In AIJ the period of the exoplanet's orbit (P) is not well constrained by the transit model, but its value will impact the best fit values of some of the fitted parameters; therefore P should be manually entered by the user. Moreover, the host star parameters are entered to estimate the transit parameters $\left(\frac{R_p}{R_*}, \frac{a}{R_*}, b \right)$. The host star radius can be retrieved from the NEA and the u_1 and u_2 are the quadratic limb darkening coefficients, which can be found by interpolation based on the stellar parameters and the passband of the observation using the limb darkening coefficient calculator for all the frequently used passbands other than the clear observations⁵. Otherwise, entering any other parameter of the host star will produce a rough estimate of R_* based on the zero age main sequence assumption (Collins et al., 2017).

Our analysis with the AIJ is more thorough in that it is based on a physical model while The ETD assumes that the planet and the host star have dark and limb-darkened disks with a radius ratio of $k = R_p / R_*$ keeping in mind that the planetary radius is much smaller than the radius of the host star, $k \leq 0.2$. The ETD uses the Levenberg-Marquardt non-linear least squares fitting algorithm (Press et al. 2007). The algorithm requires the initial values of the parameters and partial derivatives of the fitted function. For a limb-darkened star, the depth of the transit δ is

⁴ <http://astroutils.astronomy.ohio-state.edu/time/>

⁵ <http://astroutils.astronomy.ohio-state.edu/exofast/limbdark.shtml/>

determined by radius ratio k , impact factor b , and limb darkening coefficient c_1 . The ETD keeps c_1 fixed at an arbitrary value $c_1 = 0.5$ in all cases because the effect on other parameters is rather negligible, usually smaller than the error bars. The export value of the depth is then evaluated as

$$\delta = -2.5 \log [\min z F(z, k, c_1)] \quad (5)$$

z is a function with four parameters t_i , T_c , t_{14} , and b , where b is the impact parameter (Poddan'ý et al. 2009). For these reasons, we didn't use the analysis of data by ETD.

As an example of what we did in this work, the data processing with AIJ for the exoplanet HAT-P-30 b is shown in Figure 1. The raw normalized light curve and the light curve after fitting the exoplanet transit model to the data shows how the airmass detrending parameter was used to improve the fit.

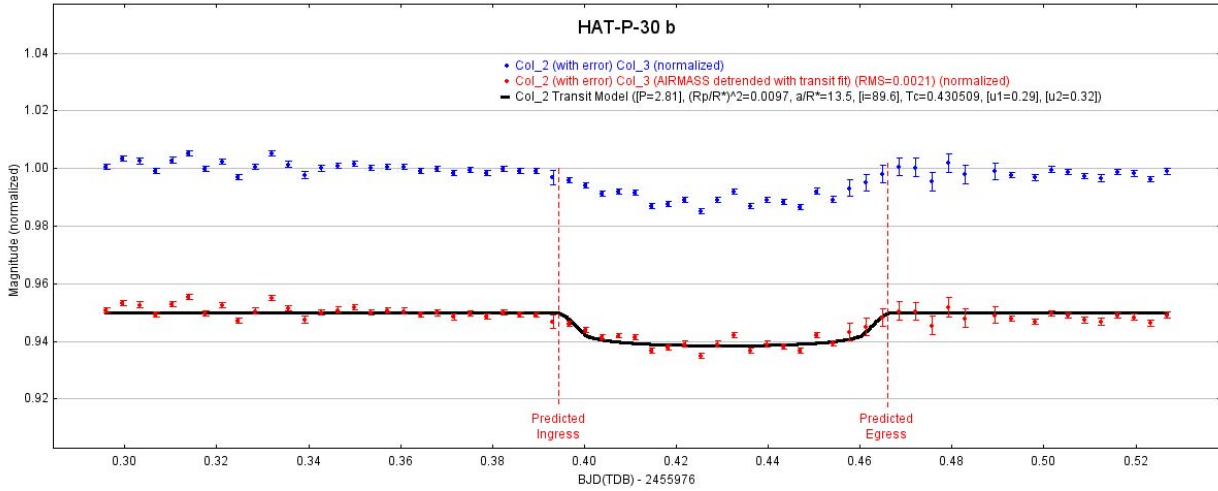


Figure 1. Multi-plot example for HAT-P-30 b transit using the airmass detrend parameter. The raw data are shown as solid blue dots which are plotted with no fit, while the solid red dots show the same data assuming that it will reflect a dip in brightness due to the exoplanet's transit, which is shown by the black line through the data.

Data Analysis

In this section, we summarize the calculation of the parameter values for each exoplanet using AIJ. Since AIJ does not find the error for each of those model parameters, uncertainties in the parameters are determined with a differential evolution MCMC simulation through a free web-based tool (EXOFAST). The EXOFAST takes flux and time (which are output of the AIJ) as input and provides parameters values in addition to the errors of some of them. This method is a standard tool in exoplanet research when the goal is to decrease the overall analysis error. Therefore, we should find the lowest χ^2 to find this minimum:

$$\chi^2 = \sum \left(\frac{D_i - M_i}{\sigma_i} \right)^2 \quad (6)$$

in which a given data set D is described by a given model M . The online EXOFAST tool is based on this method (J. Eastman et al. 2013) and has been used to derive the uncertainties only by fixing the parameter values found in the analyses⁶. With EXOFAST a set of parameters is selected and the χ^2 is evaluated for that set. Then a different set of parameters is randomly selected, the χ^2 is calculated and compared to that of the previous set to find the best set of parameters values. To do this, EXOFAST needs three columns of data including BJD_TDB, flux, flux

⁶ <http://astroutils.astronomy.ohiostate.edu/exofast/example.html>

uncertainty. Since AIJ converts magnitude to the normalized relative flux, we can derive the uncertainties in certain parameters with the help of this tool.

We listed the uncertainties of all the parameters in Tables 9-14. The tables contain the parameters of different data for every single exoplanet. Each row in these tables shows the calculated parameters for each light curve mentioned in the Data section (For example Table 9 shows all parameters calculated from 14 light curves in the HAT-P-8 b dataset). The first column is the number for each light curve of the planet; the second column (R_p) is the radius of planet in terms of the radius of Jupiter; the third column is $k = \frac{R_p}{R_*}$ which shows the ratio of the planet radius to the stellar radius; the fourth column (t_{14}) is the total transit time from the first contact to the fourth contact; the fifth column (i) is the orbital inclination (deg); the sixth column (BIC) is the BIC value. The seventh column is the mid-transit times (T_c) and other two columns are the errors FWHM duration ($\sigma_{T_{FWHM}}$), and the transit depth (σ_{depth}). We calculated the error propagation of k and R_p from the following relations:

$$\sigma_k = \frac{\sigma_{depth}}{2k}, \quad \sigma_{R_p} = k\sigma_{R_*} + R_*\sigma_k \quad (7)$$

Table 9. Parameters calculated for HAT-P-8 b

NO.	$R_p(R_j)$	k	$T_{14}(\text{day})$	$i(^{\circ})$	BIC	T_c (BJD _{TDB})	$\sigma_{T_{FWHM}}$	σ_{depth}
1	1.68 ± 0.10	0.109 ± 0.001	0.168 ± 0.002	90.0	60.31	2455034.4913 ± 0.0002	0.0018	0.00022
2	1.45 ± 0.10	0.094 ± 0.001	0.163 ± 0.002	88.6	60.00	2455046.7891 ± 0.0007	0.0015	0.00020
3	1.54 ± 0.11	0.100 ± 0.001	0.197 ± 0.003	89.9	56.06	2455071.3841 ± 0.0010	0.0021	0.00029
4	1.43 ± 0.13	0.094 ± 0.003	0.173 ± 0.008	88.8	52.42	2455071.4027 ± 0.0024	0.0049	0.00062
5	1.47 ± 0.11	0.094 ± 0.001	0.171 ± 0.004	88.2	56.50	2455071.4112 ± 0.0012	0.0024	0.00034
6	1.64 ± 0.12	0.104 ± 0.002	0.187 ± 0.007	87.6	56.74	2455071.4123 ± 0.0021	0.0043	0.00061
7	1.80 ± 0.11	0.118 ± 0.001	0.169 ± 0.004	86.0	52.93	2455074.4787 ± 0.0012	0.0024	0.00044
8	1.46 ± 0.10	0.094 ± 0.000	0.169 ± 0.001	88.3	51.70	2455437.4888 ± 0.0003	0.00072	0.00010
9	1.75 ± 0.11	0.114 ± 0.001	0.156 ± 0.004	88.0	48.44	2455437.4897 ± 0.0012	0.0024	0.00042
10	1.46 ± 0.11	0.094 ± 0.001	0.166 ± 0.004	88.6	41.90	2455440.5651 ± 0.0012	0.0024	0.00036
11	1.39 ± 0.10	0.089 ± 0.001	0.176 ± 0.002	88.4	50.56	2455452.8620 ± 0.0008	0.0016	0.00020
12	1.47 ± 0.10	0.094 ± 0.001	0.166 ± 0.002	88.3	42.19	2455800.4924 ± 0.0007	0.0015	0.00024
13	1.43 ± 0.10	0.094 ± 0.000	0.167 ± 0.001	88.2	50.89	2456175.8100 ± 0.0005	0.0010	0.00014
14	1.22 ± 0.11	0.077 ± 0.001	0.150 ± 0.001	88.5	51.06	2457615.5360 ± 0.0011	0.0021	0.00028

Table 10. Parameters calculated for HAT-P-16 b

NO.	$R_p(R_j)$	k	$T_{14}(\text{day})$	$i(^{\circ})$	BIC	T_c (BJD _{TDB})	$\sigma_{T_{FWHM}}$	σ_{depth}
1	1.19 ± 0.05	0.099 ± 0.001	0.1287 ± 0.0021	88.4	45.75	2455463.4190 ± 0.0006	0.0012	0.00026
2	1.46 ± 0.05	0.121 ± 0.001	0.1263 ± 0.0003	88.5	66.40	2455463.4204 ± 0.0001	0.00021	0.00029
3	1.29 ± 0.05	0.107 ± 0.001	0.1231 ± 0.0004	88.0	61.78	2455482.8513 ± 0.0001	0.00024	0.00028
4	1.34 ± 0.05	0.112 ± 0.000	0.1300 ± 0.0002	88.0	70.64	2455829.8521 ± 0.0002	0.00012	0.00016
5	1.20 ± 0.06	0.101 ± 0.002	0.1245 ± 0.0024	88.6	53.79	2455835.3994 ± 0.0007	0.0014	0.00045
6	1.34 ± 0.06	0.112 ± 0.001	0.1236 ± 0.0005	88.3	55.34	2455835.4019 ± 0.0001	0.00034	0.00042
7	1.29 ± 0.05	0.107 ± 0.001	0.1270 ± 0.0001	89.0	65.40	2455843.7303 ± 0.0003	0.00022	0.00030
8	1.19 ± 0.06	0.099 ± 0.001	0.1312 ± 0.0004	89.1	52.10	2455935.3303 ± 0.0001	0.00024	0.00033
9	1.58 ± 0.23	0.131 ± 0.024	0.1442 ± 0.0071	87.4	50.33	2456218.4696 ± 0.0020	0.00414	0.00633
10	1.55 ± 0.05	0.129 ± 0.001	0.1231 ± 0.0006	88.0	57.83	2456540.4996 ± 0.0002	0.00040	0.00047
11	1.33 ± 0.05	0.111 ± 0.001	0.1251 ± 0.0002	88.5	65.93	2456601.5685 ± 0.0002	0.00016	0.00022
12	1.26 ± 0.06	0.105 ± 0.001	0.1263 ± 0.0006	89.0	60.69	2456604.3436 ± 0.0001	0.00036	0.00041
13	1.39 ± 0.05	0.116 ± 0.001	0.1211 ± 0.0009	89.0	62.18	2456629.3272 ± 0.0002	0.00055	0.00041
14	1.49 ± 0.05	0.124 ± 0.001	0.1302 ± 0.0005	88.7	53.96	2457334.4231 ± 0.0001	0.00029	0.00038
15	1.30 ± 0.05	0.108 ± 0.002	0.1257 ± 0.0004	89.9	49.25	2457345.5264 ± 0.0001	0.00025	0.00043
16	1.21 ± 0.05	0.100 ± 0.001	0.1248 ± 0.0004	88.4	50.77	2457706.4042 ± 0.0001	0.00023	0.00023

Table 11. Parameters calculated for HAT-P-21 b

NO.	$R_p(R_j)$	K	$T_{14}(\text{day})$	$i(^{\circ})$	BIC	T_c (BJD _{TDB})	$\sigma_{T_{FWHM}}$	σ_{depth}
1	1.08 ± 0.18	0.100 ± 0.002	0.1532 ± 0.0010	88.6	56.04	2455627.4771 ± 0.0002	0.00059	0.00053
2	1.10 ± 0.17	0.102 ± 0.001	0.1701 ± 0.0006	88.5	50.09	2455660.4595 ± 0.0001	0.00037	0.00034
3	1.04 ± 0.18	0.096 ± 0.002	0.1504 ± 0.0007	88.8	52.29	2455928.5470 ± 0.0002	0.00042	0.00045
4	1.09 ± 0.17	0.102 ± 0.001	0.1531 ± 0.0004	88.5	67.15	2456699.8261 ± 0.0001	0.00025	0.00028

5	0.98 ± 0.19	0.091 ± 0.002	0.1438 ± 0.0010	88.7	49.38	2457516.4663 ± 0.0002	0.00059	0.00053
---	-----------------	-------------------	---------------------	------	-------	---------------------------	---------	---------

Table 12. Parameters calculated for HAT-P-22 b

NO.	$R_p(R_i)$	K	$T_{14}(\text{day})$	$i(^{\circ})$	BIC	$T_c(\text{BJD}_{\text{TDB}})$	$\sigma_{T_{FWHM}}$	σ_{depth}
1	0.94 ± 0.06	0.093 ± 0.001	0.1164 ± 0.0004	88.5	57.18	2455614.4272 ± 0.0001	0.00026	0.00032
2	1.05 ± 0.06	0.103 ± 0.001	0.1201 ± 0.0002	90.0	50.48	2455630.4828 ± 0.0002	0.00024	0.00029
3	1.08 ± 0.07	0.107 ± 0.002	0.1211 ± 0.0005	88.4	44.67	2455948.4979 ± 0.0001	0.00033	0.00052
4	1.05 ± 0.06	0.104 ± 0.001	0.1164 ± 0.0005	88.8	65.26	2456327.5369 ± 0.0001	0.00030	0.00026
5	1.12 ± 0.05	0.111 ± 0.001	0.1221 ± 0.0002	85.8	59.55	2456356.4504 ± 0.0006	0.00013	0.00021
6	1.02 ± 0.05	0.101 ± 0.001	0.1161 ± 0.0002	88.5	65.78	2456687.3126 ± 0.0001	0.00014	0.00019
7	1.07 ± 0.06	0.106 ± 0.001	0.1142 ± 0.0002	89.1	55.83	2456780.4644 ± 0.0002	0.00022	0.00037
8	1.08 ± 0.29	0.107 ± 0.024	0.0906 ± 0.0062	88.8	51.40	2457024.5856 ± 0.0018	0.00362	0.00513
9	1.16 ± 0.20	0.115 ± 0.015	0.1278 ± 0.0037	88.9	57.19	2457024.5971 ± 0.0010	0.00218	0.00364
10	1.13 ± 0.05	0.112 ± 0.001	0.1202 ± 0.0001	88.7	73.29	2457734.5013 ± 0.0002	0.00011	0.00015
11	1.08 ± 0.07	0.107 ± 0.002	0.1156 ± 0.0005	88.8	46.41	2457779.4723 ± 0.0001	0.00030	0.00049

Table 13. Parameters calculated for HAT-P-28 b

NO.	$R_p(R_i)$	k	$T_{14}(\text{day})$	$i(^{\circ})$	BIC	$T_c(\text{BJD}_{\text{TDB}})$	$\sigma_{T_{FWHM}}$	σ_{depth}
1	1.42 ± 0.09	0.130 ± 0.002	0.138 ± 0.004	87.3	62.50	2455808.4618 ± 0.0012	0.0024	0.00059
2	1.16 ± 0.11	0.109 ± 0.003	0.101 ± 0.005	90,0	60.28	2455808.4753 ± 0.0015	0.0030	0.00084
3	1.43 ± 0.09	0.134 ± 0.002	0.136 ± 0.004	90,0	45.85	2455808.4718 ± 0.0013	0.0026	0.00076
4	1.34 ± 0.08	0.126 ± 0.001	0.115 ± 0.002	89.4	47.28	2455808.4717 ± 0.0007	0.0014	0.00045
5	1.28 ± 0.09	0.118 ± 0.002	0.150 ± 0.004	89.5	41.59	2455834.5225 ± 0.0012	0.0025	0.00065
6	1.36 ± 0.09	0.126 ± 0.003	0.130 ± 0.006	89.9	43.82	2455834.5199 ± 0.0017	0.0034	0.00076
7	1.18 ± 0.09	0.109 ± 0.002	0.127 ± 0.001	88.4	56.21	2455834.5251 ± 0.0021	0.0022	0.00052
8	1.11 ± 0.10	0.104 ± 0.002	0.121 ± 0.004	88.4	55.12	2455857.3183 ± 0.0012	0.0025	0.00053
9	1.20 ± 0.09	0.114 ± 0.001	0.137 ± 0.003	88.2	55.76	2455912.6913 ± 0.0009	0.0019	0.00039
10	1.19 ± 0.08	0.109 ± 0.001	0.132 ± 0.003	88.4	54.03	2456508.7671 ± 0.0009	0.0019	0.00040
11	1.20 ± 0.09	0.109 ± 0.002	0.127 ± 0.003	88.9	57.10	2456609.7361 ± 0.0009	0.0019	0.00046
12	1.32 ± 0.09	0.122 ± 0.001	0.136 ± 0.004	88.5	59,00	2456658.5958 ± 0.0013	0.0026	0.00048
13	1.06 ± 0.09	0.100 ± 0.001	0.131 ± 0.003	89.1	49.27	2456886.6009 ± 0.0009	0.0018	0.00039
14	1.17 ± 0.08	0.109 ± 0.001	0.128 ± 0.003	89.8	57.69	2456902.8861 ± 0.0004	0.0015	0.00028
15	1.61 ± 0.08	0.151 ± 0.000	0.131 ± 0.002	89.9	53.28	2457010.3742 ± 0.0005	0.0011	0.00025
16	1.23 ± 0.10	0.114 ± 0.003	0.134 ± 0.006	87.4	46.35	2457326.3225 ± 0.0017	0.0034	0.00076
17	1.21 ± 0.11	0.114 ± 0.004	0.130 ± 0.007	88.3	52.83	2457684.6190 ± 0.0022	0.0044	0.00100
18	1.26 ± 0.08	0.118 ± 0.000	0.136 ± 0.001	89.9	47.00	2457710.6781 ± 0.0002	0.00049	0.00017
19	1.38 ± 0.10	0.130 ± 0.003	0.138 ± 0.007	86.2	54.56	2458404.4685 ± 0.0020	0.0041	0.00102
20	1.25 ± 0.09	0.118 ± 0.002	0.134 ± 0.004	88.6	49.70	2458479.3831 ± 0.0012	0.0024	0.00059

Table 14. Parameters calculated for HAT-P-30 b

NO.	$R_p(R_i)$	k	$T_{14}(\text{day})$	$i(^{\circ})$	BIC	$T_c(\text{BJD}_{\text{TDB}})$	$\sigma_{T_{FWHM}}$	σ_{depth}
1	1.43 ± 0.12	0.109 ± 0.002	0.080 ± 0.004	85.1	41.74	2455650.3980 ± 0.0011	0.0023	0.00061
2	1.24 ± 0.12	0.094 ± 0.002	0.070 ± 0.004	89.6	57.20	2455894.9223 ± 0.0012	0.0025	0.00046
3	1.32 ± 0.12	0.100 ± 0.002	0.079 ± 0.003	88.5	49.35	2455945.5112 ± 0.0008	0.0017	0.00044
4	1.40 ± 0.32	0.104 ± 0.024	0.082 ± 0.007	88.6	59.30	2455970.8145 ± 0.0021	0.0042	0.00513
5	1.18 ± 0.11	0.089 ± 0.001	0.081 ± 0.009	86.2	52.88	2455976.4272 ± 0.0026	0.0052	0.00034
6	1.41 ± 0.12	0.109 ± 0.002	0.084 ± 0.004	83.4	41.59	2455976.4299 ± 0.0012	0.0025	0.00055
7	1.36 ± 0.11	0.104 ± 0.002	0.061 ± 0.002	88.6	57.78	2456001.7266 ± 0.0008	0.0015	0.00045
8	1.48 ± 0.19	0.114 ± 0.010	0.126 ± 0.008	79.6	48.04	2456240.6226 ± 0.0024	0.0049	0.0023
9	1.26 ± 0.13	0.094 ± 0.003	0.071 ± 0.003	89.6	57.56	2456296.8374 ± 0.0008	0.0017	0.00061
10	1.24 ± 0.12	0.094 ± 0.002	0.086 ± 0.004	88.3	49.63	2456687.5067 ± 0.0012	0.0024	0.00055
11	1.29 ± 0.11	0.100 ± 0.001	0.090 ± 0.003	85.0	43.57	2456704.3739 ± 0.0009	0.0019	0.00036
12	1.37 ± 0.27	0.104 ± 0.018	0.097 ± 0.004	87.1	57.16	2456735.2853 ± 0.0012	0.0024	0.0039
13	1.33 ± 0.11	0.104 ± 0.001	0.057 ± 0.003	89.6	57.00	2456982.6255 ± 0.0007	0.0016	0.00039
14	1.20 ± 0.11	0.089 ± 0.001	0.076 ± 0.003	86.8	52.22	2457013.5430 ± 0.0010	0.0021	0.00034
15	1.46 ± 0.11	0.114 ± 0.001	0.092 ± 0.003	83.6	35.83	2458140.5902 ± 0.0008	0.0017	0.00039
16	1.45 ± 0.11	0.114 ± 0.001	0.092 ± 0.002	83.1	41.90	2458528.4551 ± 0.0007	0.0015	0.00035

Conclusion

In order to check the light curves of the six planets for which an initial analysis was made using ETD, we examined an independent software package (AIJ) and denoted the reason for using it in the Method section. In the Data Analysis section, we studied a total of 82 light curves and extracted parameters from them such as R_p , k , t_{14} , T_c and i and have tabulated them along with their uncertainties in Tables 9-14. In order to analyze the light curves recorded in the same passband, we plotted them in units of relative flux with respect to the orbital phase for each of the passbands. Then we analyzed the data with the same filter using AIJ (Table 16). The light curves related to special filters have mentioned (Appendix B.). Then we analyzed the data with the same filter using AIJ. The Precise values of the parameters show that using AIJ as a fitting tool for follow-up observations can lead to results comparable to the NEA (Table 15). The similarities in the parameter values show the merit in analysis of amateur data by making use of the right software packages such as AstrolmageJ and web services as EXOFAST, considering the differences in the qualities of photometric data acquired by amateur observers and the precise follow-up light curves from relatively larger telescopes to derive the parameters given in the literature. They also prove the follow-up potential of amateur and university observatories in providing system parameters as well as mid-transit times. Such information will be invaluable considering the numbers of future discoveries from the ground and space-based exoplanet surveys.

Table 15. Specifications of planets and their host stars (NASA Exoplanet Archive)

Planets	$R_p(R_j)$	k	$t_{14}(\text{day})$	i (deg)	T_c (BJD _{TDB})	R_* (R_{sun})	L_* ($\log_{10}(L_{\text{sun}})$)	M_* (M_{sun})
HAT-P-8 b	1.40 ± 0.13 (Stassun et al. 2017)	0.0953 ± 0.0009 (Latham et al. 2009)	0.1587 ± 0.0011 (Latham et al. 2009)	87.8 ± 0.76 (Stassun et al. 2017)	2454437.6749 ± 0.0014 (Bonomo et al. 2017)	1.57 ± 0.15 (Stassun et al. 2017)	0.5190 ± 0.050 (Latham et al. 2009)	1.27 ± 0.41 (Stassun et al. 2017)
HAT-P-16 b	1.289 ± 0.066 (Buchhave et al. 2010)	0.1071 ± 0.0014 (Buchhave et al. 2010)	0.1276 ± 0.0013 (Buchhave et al. 2010)	86.6 ± 0.7 (Buchhave et al. 2010)	$2455027.59293 \pm 0.00031$ (Buchhave et al. 2010)	1.24 ± 0.054 (Buchhave et al. 2010)	$0.294^{+0.046}_{-0.051}$ (Buchhave et al. 2010)	1.22 ± 0.039 (Buchhave et al. 2010)
HAT-P-21 b	1.11 ± 0.16 (Stassun et al. 2017)	0.0950 ± 0.0022 (Bakos et al. 2011)	0.1530 ± 0.0027 (Bakos et al. 2011)	87.2 ± 0.70 (Stassun et al. 2017)	$2454996.41312 \pm 0.00069$ (Bakos et al. 2011)	1.21 ± 0.17 (Stassun et al. 2017)	$0.1481^{+0.007184}_{-0.007304}$ (Brown et al. 2018)	1.24 ± 0.60 (Stassun et al. 2017)
HAT-P-22 b	1.15 ± 0.19 (Stassun et al. 2017)	0.1065 ± 0.0017 (Turner et al. 2016)	0.1196 ± 0.0014 (Bakos et al. 2011)	86.9 ± 0.55 (Stassun et al. 2017)	$2454930.22001 \pm 0.00025$ (Bakos et al. 2011)	1.11 ± 0.05 (Stassun et al. 2017)	$-0.114^{+0.048}_{-0.054}$ (Bakos et al. 2011)	1.13 ± 0.22 (Stassun et al. 2017)
HAT-P-28 b	$1.212^{+0.113}_{-0.082}$ (Buchhave et al. 2011)	0.1130 ± 0.0024 (Buchhave et al. 2011)	0.1341 ± 0.0020 (Buchhave et al. 2011)	88.0 ± 0.9 (Buchhave et al. 2011)	$2455417.59832 \pm 0.00053$ (Buchhave et al. 2011)	$1.10^{+0.091}_{-0.069}$ (Buchhave et al. 2011)	$0.053^{+0.080}_{-0.066}$ (Buchhave et al. 2011)	1.03 ± 0.047 (Buchhave et al. 2011)
HAT-P-30 b	1.44 ± 0.15 (Stassun et al. 2017)	$0.1109^{+0.0016}_{-0.0014}$ (Maciejewski et al. 2016)	0.0887 ± 0.0015 (Johnson et al. 2011)	83.6 ± 0.04 (Stassun et al. 2017)	$2455456.46561 \pm 0.00037$ (Johnson et al. 2011)	1.31 ± 0.13 (Stassun et al. 2017)	$0.4097^{+0.00615}_{-0.00623}$ (Brown et al. 2018)	1.55 ± 0.51 (Stassun et al. 2017)

Table 16. AIJ's results with the same filter

Planets	$R_p(R_j)$	k	$t_{14}(\text{day})$	i (deg)
HAT-P-8 b (R)	1.41 ± 0.12	0.0943 ± 0.0019	0.1653 ± 0.0012	89.4
HAT-P-8 b (Clear)	1.46 ± 0.11	0.0959 ± 0.0017	0.1634 ± 0.0035	89.9
HAT-P-16 b (R)	1.29 ± 0.05	0.1077 ± 0.0014	0.1251 ± 0.0010	89.6
HAT-P-16 b (V)	1.33 ± 0.05	0.1109 ± 0.0017	0.1271 ± 0.0009	89.8
HAT-P-16 b (I)	1.20 ± 0.06	0.0994 ± 0.0018	0.1326 ± 0.0006	89.3
HAT-P-16b (Clear)	1.31 ± 0.06	0.1224 ± 0.0019	0.1343 ± 0.0023	88.6
HAT-P-21 b (R)	1.17 ± 0.16	0.0994 ± 0.0023	0.1559 ± 0.0004	89.7
HAT-P-21 b (Clear)	1.11 ± 0.16	0.0948 ± 0.0023	0.1484 ± 0.0007	89.9
HAT-P-22 b (R)	1.16 ± 0.06	0.1072 ± 0.0017	0.1194 ± 0.0007	89.7
HAT-P-22 b (V)	1.10 ± 0.06	0.1019 ± 0.0021	0.1175 ± 0.0005	89.5
HAT-P-22 b (Clear)	1.11 ± 0.06	0.1034 ± 0.0015	0.1149 ± 0.0002	89.4

HAT-P-28 b (R)	1.25 ± 0.09	0.1170 ± 0.0022	0.1361 ± 0.0037	89.9
HAT-P-28 b (Clear)	1.25 ± 0.09	0.1178 ± 0.0027	0.1296 ± 0.0032	89.9
HAT-P-30 b (R)	1.41 ± 0.27	0.1113 ± 0.0186	0.0868 ± 0.0041	87.5
HAT-P-30 b (V)	1.31 ± 0.29	0.1029 ± 0.0195	0.0888 ± 0.0038	89.9
HAT-P-30 b (I)	1.25 ± 0.28	0.0979 ± 0.0180	0.0899 ± 0.0053	89.6
HAT-P-30 b (Clear)	1.38 ± 0.26	0.1063 ± 0.0175	0.0916 ± 0.0031	87.3

Acknowledgements

This manuscript was prepared by the International Occultation Timing Association Middle East section (IOTA/ME). We would like to thank the local and scientific organizers of the IOTA/ME Photometric Observations of Exoplanet Transits Workshop held in Ankara University between 13-18 October 2018 for the hands-on exercises in exoplanet transit analyses.

References

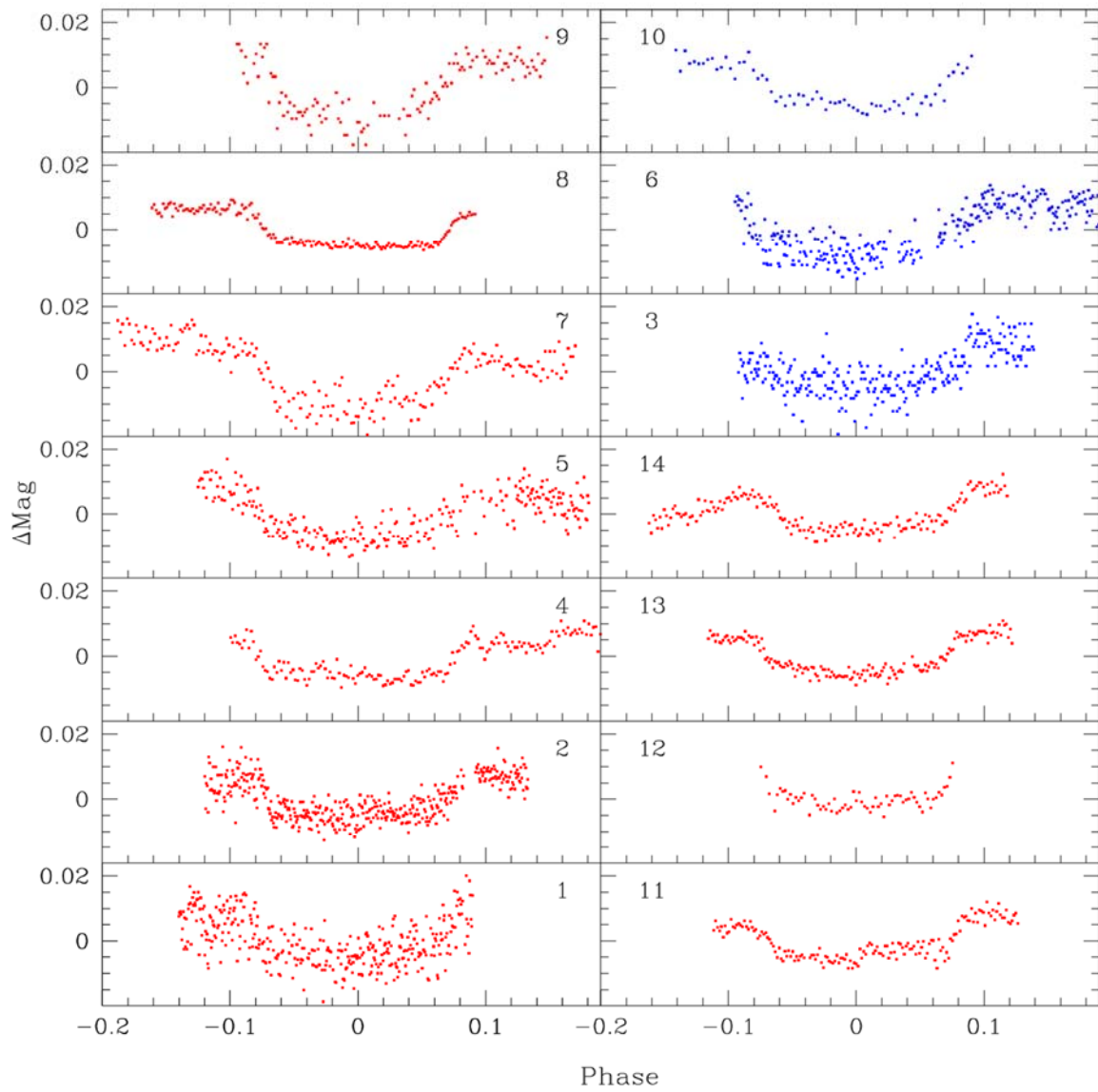
- Bakos, G., Noyes, R. W., Kovács, G., Stanek, K. Z., Sasselov, D. D., Domsa, I. 2004. "Wide- Field Milli magnitude Photometry with the HAT: A Tool for Extrasolar Planet Detection", *The Publications of the Astronomical Society of the Pacific*, 116, 266
- Bakos, G.Á., 2018. The HATNet and HATSouth Exoplanet Surveys. *arXiv preprint arXiv:1801.00849*.
- Poddaný, S., Brát, L. and Pejcha, O., 2010. Exoplanet Transit Database. Reduction and processing of the photometric data of exoplanet transits. *New Astronomy*, 15(3), pp.297-301.
- Mandel, K. and Agol, E., 2002. Analytic light curves for planetary transit searches. *The Astrophysical Journal Letters*, 580(2), p.L171.
- Collins, K.A., Kielkopf, J.F., Stassun, K.G. and Hessman, F.V., 2017. AstromageJ: Image Processing and Photometric Extraction for Ultra-Precise Astronomical Light Curves (Expanded Edition). *arXiv preprint arXiv:1701.04817*.
- Akeson, R.L., Chen, X., Ciardi, D., Crane, M., Good, J., Harbut, M., Jackson, E., Kane, S.R., Laity, A.C., Leifer, S. and Lynn, M., 2013. The NASA exoplanet archive: data and tools for exoplanet research. *Publications of the Astronomical Society of the Pacific*, 125(930), p.989.
- Latham, D.W., Bakos, G.Á., Torres, G., Stefanik, R.P., Noyes, R.W., Kovács, G., Pál, A., Marcy, G.W., Fischer, D.A., Butler, R.P. and Sipőcz, B., 2009. Discovery of a transiting planet and eight eclipsing binaries in HATNet field G205. *The Astrophysical Journal*, 704(2), p.1107.
- Buchhave, L.A., Bakos, G.Á., Hartman, J.D., Torres, G., Kovács, G., Latham, D.W., Noyes, R.W., Esquerdo, G.A., Everett, M., Howard, A.W. and Marcy, G.W., 2010. HAT-P-16b: A 4 Mj Planet Transiting A Bright Star On An Eccentric Orbit. *The Astrophysical Journal*, 720(2), p.1118.
- Hog, E., Fabricius, C., Makarov, V.V., Urban, S., Corbin, T., Wycoff, G., Bastian, U., Schwekendiek, P. and Wicenec, A., 2000. *The Tycho-2 catalogue of the 2.5 million brightest stars*. NAVAL OBSERVATORY WASHINGTON DC.
- Cutri, R.M., Skrutskie, M.F., Van Dyk, S., Beichman, C.A., Carpenter, J.M., Chester, T., Cambresy, L., Evans, T., Fowler, J., Gizis, J. and Howard, E., 2003. 2MASS All Sky Catalog of point sources, The IRSA 2MASS All-Sky Point Source Catalog, NASA/IPAC Infrared Science Archive.
- Johnson, J.A., Winn, J.N., Bakos, G.Á., Hartman, J.D., Morton, T.D., Torres, G., Kovács, G., Latham, D.W., Noyes, R.W., Sato, B. and Esquerdo, G.A., 2011. HAT-P-30b: a transiting hot Jupiter on a highly oblique orbit. *The Astrophysical Journal*, 735(1), p.24.
- Eastman, J., Siverd, R. and Gaudi, B.S., 2010. Achieving better than 1 minute accuracy in the heliocentric and barycentric Julian dates. *Publications of the Astronomical Society of the Pacific*, 122(894), p.935.
- Bentler, P.M., 1995. *EQS structural equations program manual*(Vol. 6). Encino, CA: Multivariate software.

- Press, W.H., Teukolsky, S.A., Vetterling, W.T. and Flannery, B.P., 2007. *Numerical recipes 3rd edition: The art of scientific computing*. Cambridge university press.
- Eastman, J., Gaudi, B.S. and Agol, E., 2013. EXOFAST: a fast exoplanetary fitting suite in IDL. *Publications of the Astronomical Society of the Pacific*, 125(923), p.83.
- Stassun, K.G., Collins, K.A. and Gaudi, B.S., 2017. Accurate empirical radii and masses of planets and their host stars with Gaia parallaxes. *The Astronomical Journal*, 153(3), p.136.
- Bonomo, A.S., Desidera, S., Benatti, S., Borsa, F., Crespi, S., Damasso, M., Lanza, A.F., Sozzetti, A., Lodato, G., Marzari, F. and Boccato, C., 2017. The GAPS Programme with HARPS-N at TNG-XIV. Investigating giant planet migration history via improved eccentricity and mass determination for 231 transiting planets. *Astronomy & Astrophysics*, 602, p.A107.
- Bakos, G.Á., Hartman, J., Torres, G., Latham, D.W., Kovács, G., Noyes, R.W., Fischer, D.A., Johnson, J.A., Marcy, G.W., Howard, A.W. and Kipping, D., 2011. HAT-P-20b–HAT-P-23b: Four massive transiting extrasolar planets. *The Astrophysical Journal*, 742(2), p.116.
- Brown, A.G.A., Vallenari, A., Prusti, T., De Bruijne, J.H.J., Babusiaux, C., Bailer-Jones, C.A.L., Biermann, M., Evans, D.W., Eyer, L., Jansen, F. and Jordi, C., 2018. Gaia Data Release 2-Summary of the contents and survey properties. *Astronomy & astrophysics*, 616, p.A1.
- Turner, J.D., Pearson, K.A., Biddle, L.I., Smart, B.M., Zellem, R.T., Teske, J.K., Hardegree-Ullman, K.K., Griffith, C.C., Leiter, R.M., Cates, I.T. and Nieberding, M.N., 2016. Ground-based near-UV observations of 15 transiting exoplanets: constraints on their atmospheres and no evidence for asymmetrical transits. *Monthly Notices of the Royal Astronomical Society*, 459(1), pp.789-819.
- Maciejewski, G., Dimitrov, D., Mancini, L., Southworth, J., Ciceri, S., D'Ago, G., Bruni, I., Raetz, S., Nowak, G., Ohlert, J. and Puchalski, D., 2016. New transit observations for HAT-P-30 b, HAT-P-37 b, TrES-5 b, WASP-28 b, WASP-36 b, and WASP-39 b. *arXiv preprint arXiv:1603.03268*.

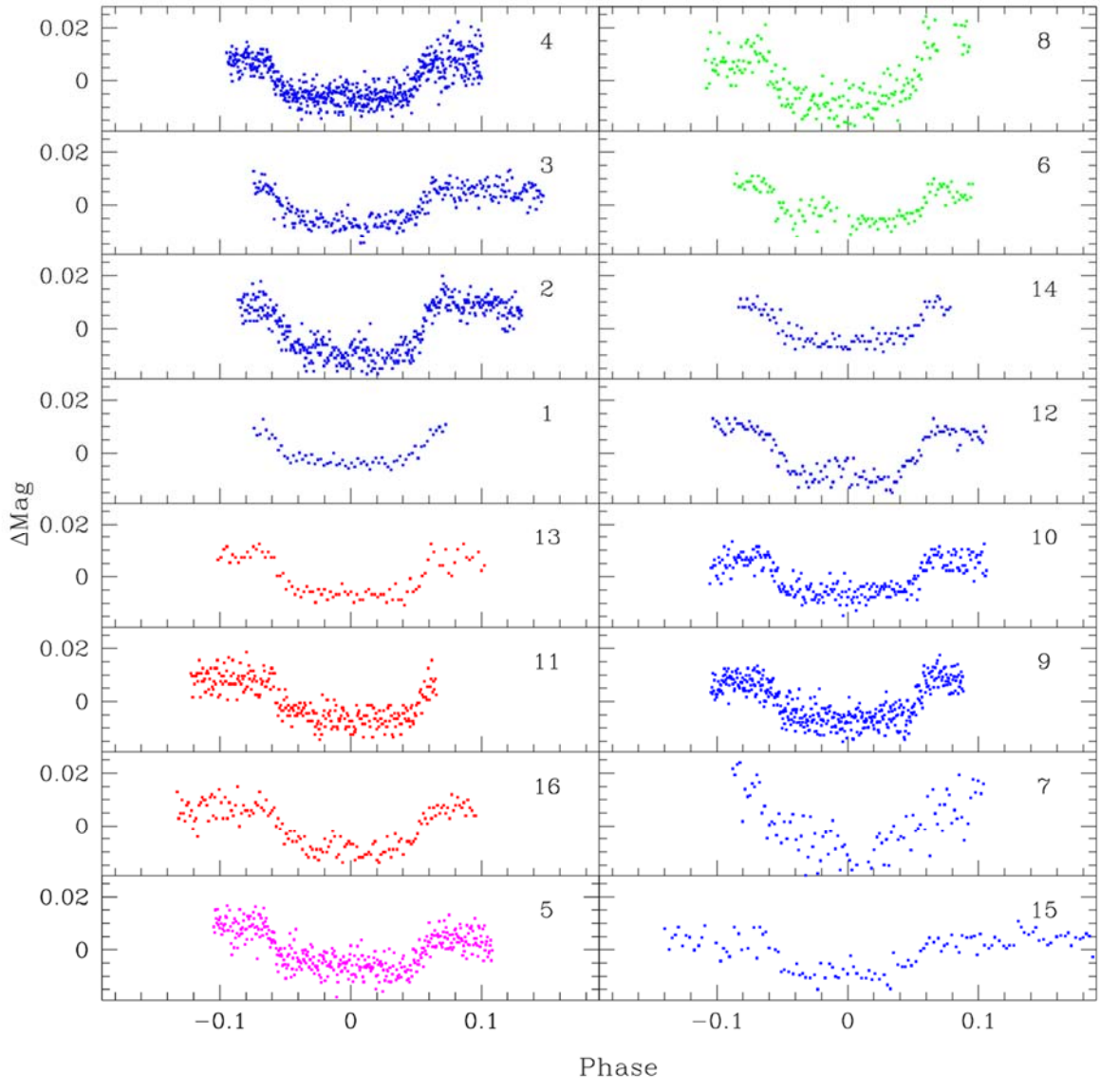
Appendix A.

In figures A1-A6, the horizontal axis is plotted based on the mid-point of the transit and the zero point in the graph is equal to T_c based on BJD. The vertical axis is based on delta magnitude of the star and the zero point is the mean of average of delta magnitude.

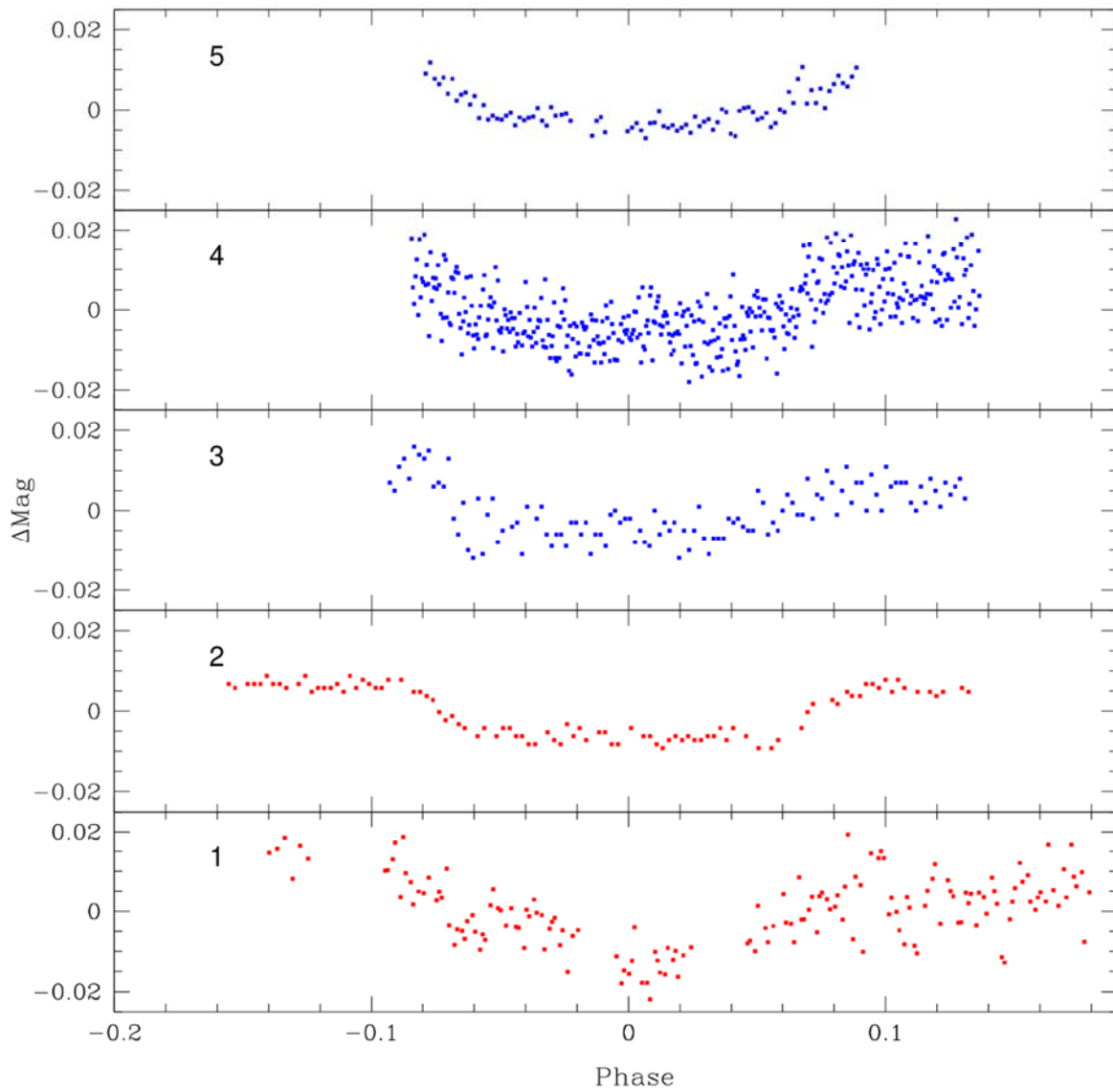
The pink color signifies that the light curve was made using an I filter; the red color denotes an R filter; blue color denotes the Clear filter, and the green color, the V filter. Each graph is marked with a number according to the Tables 2-7.



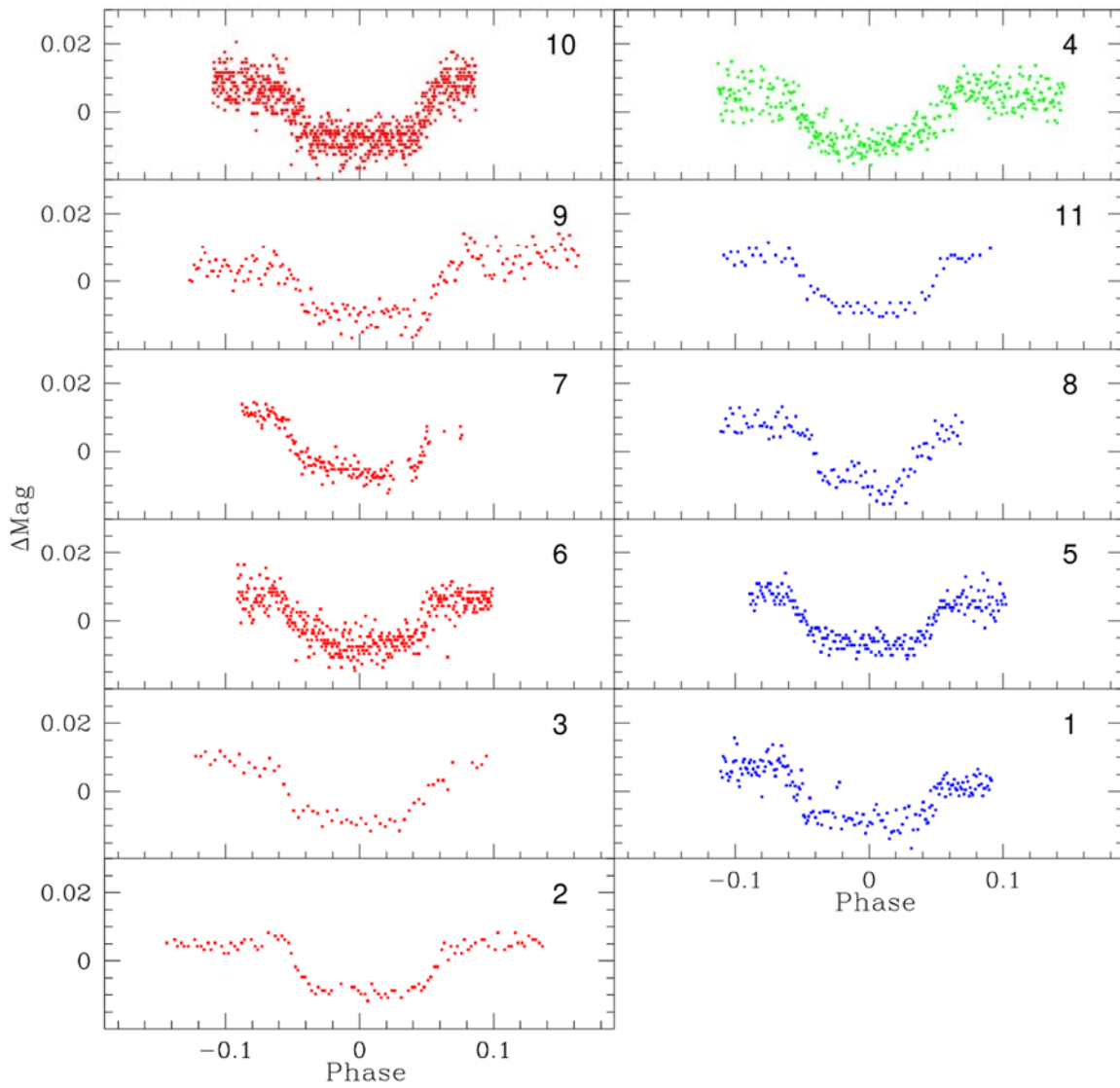
A1. Light curves of Planet HAT-P-8 b



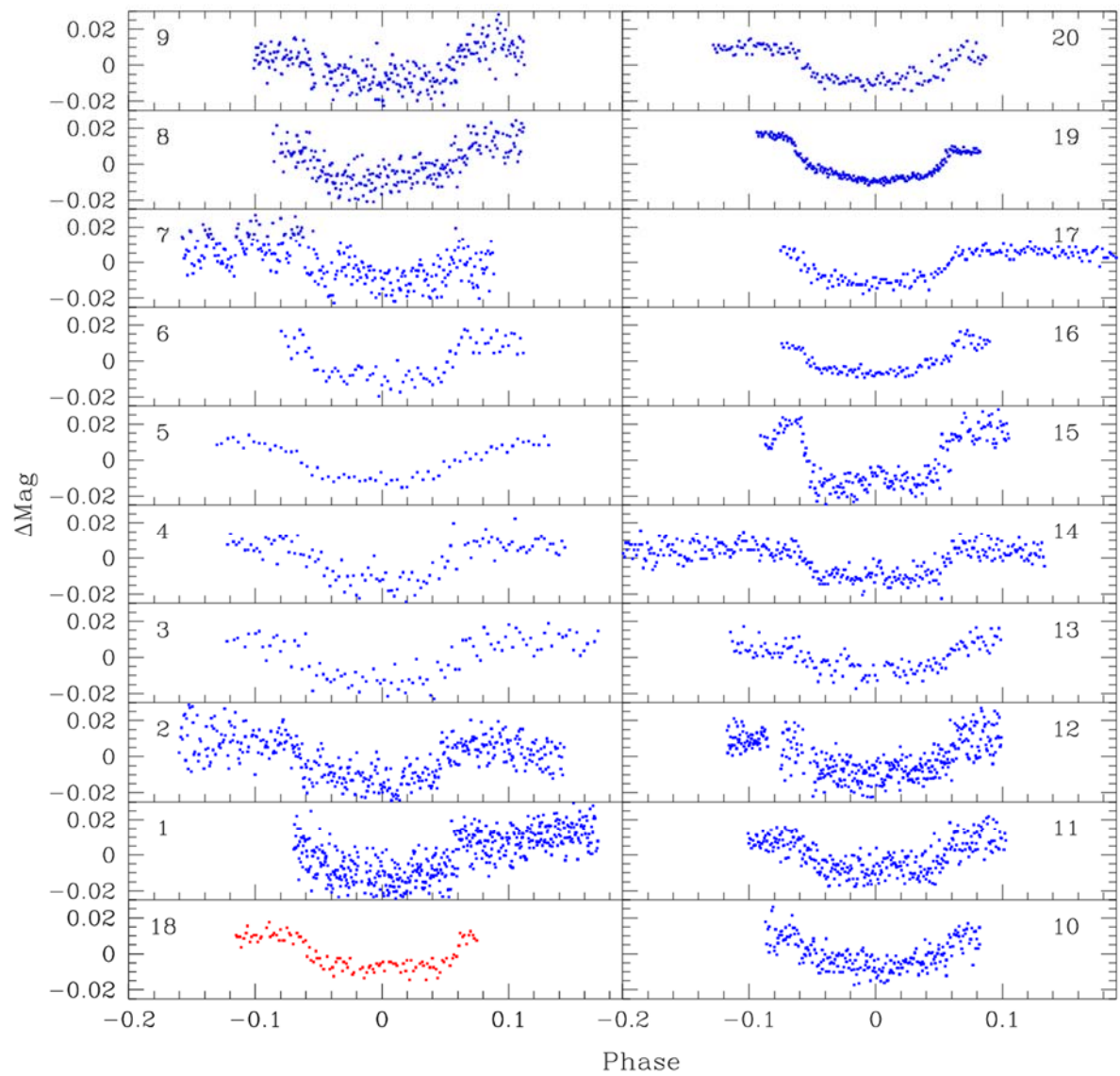
A2. Light curves of Planet HAT-P-16 b



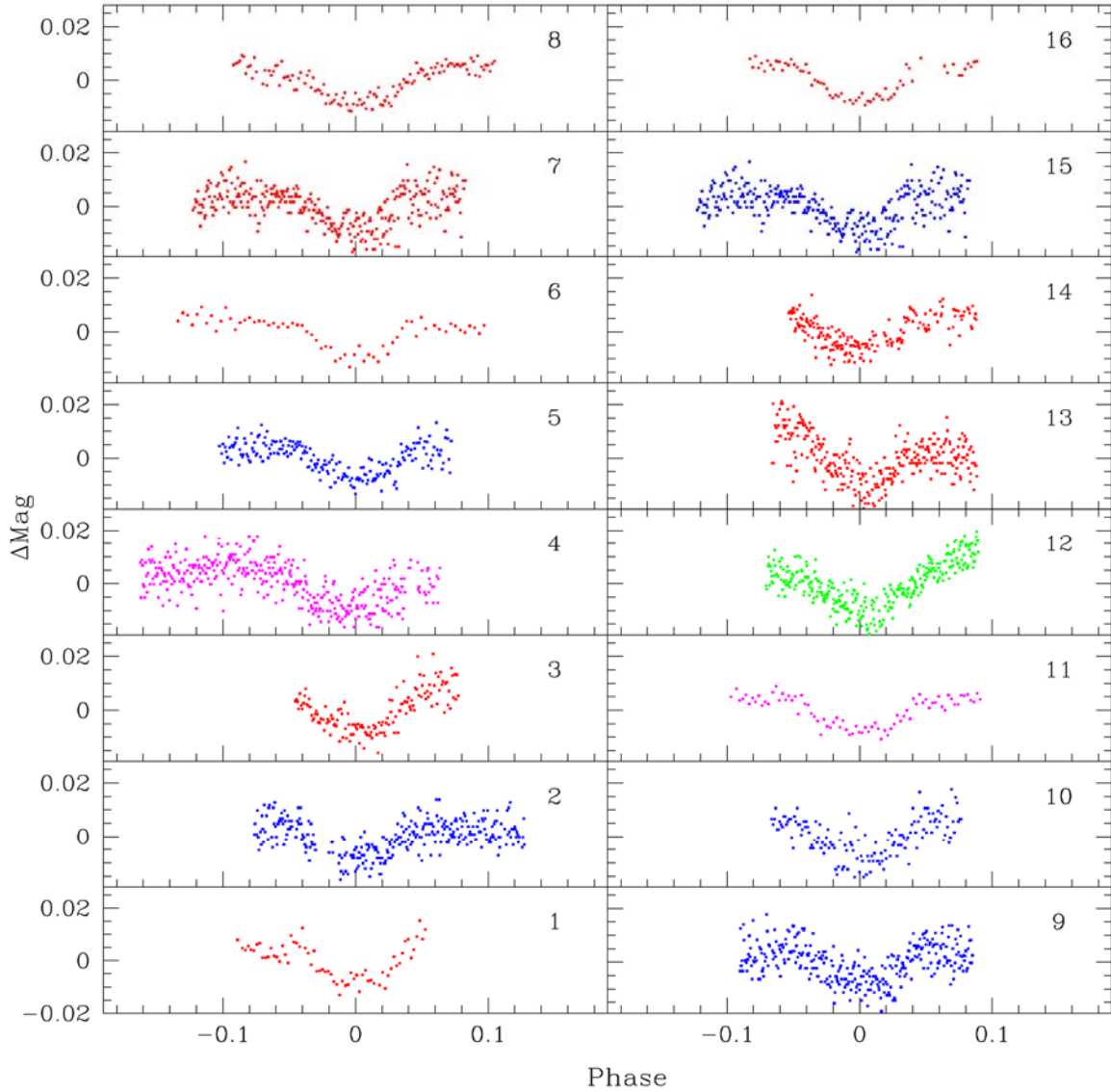
A3. Light curves of Planet HAT-P-21 b



A4. Light curves of Planet HAT-P-22 b



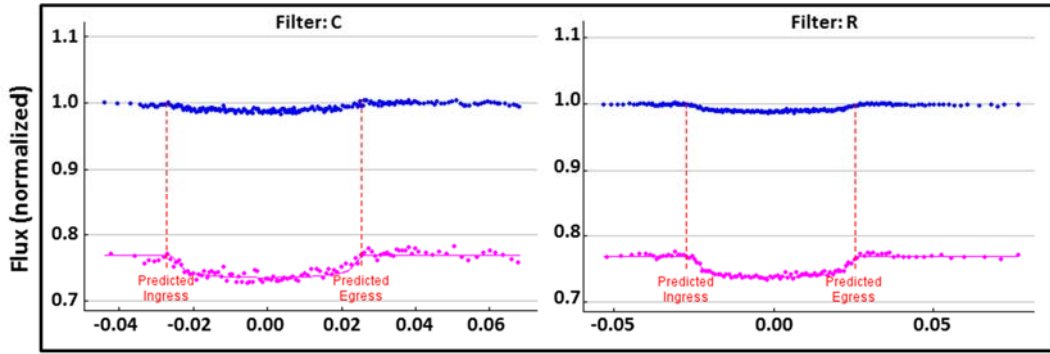
A5. Light curves of Planet HAT-P-28 b



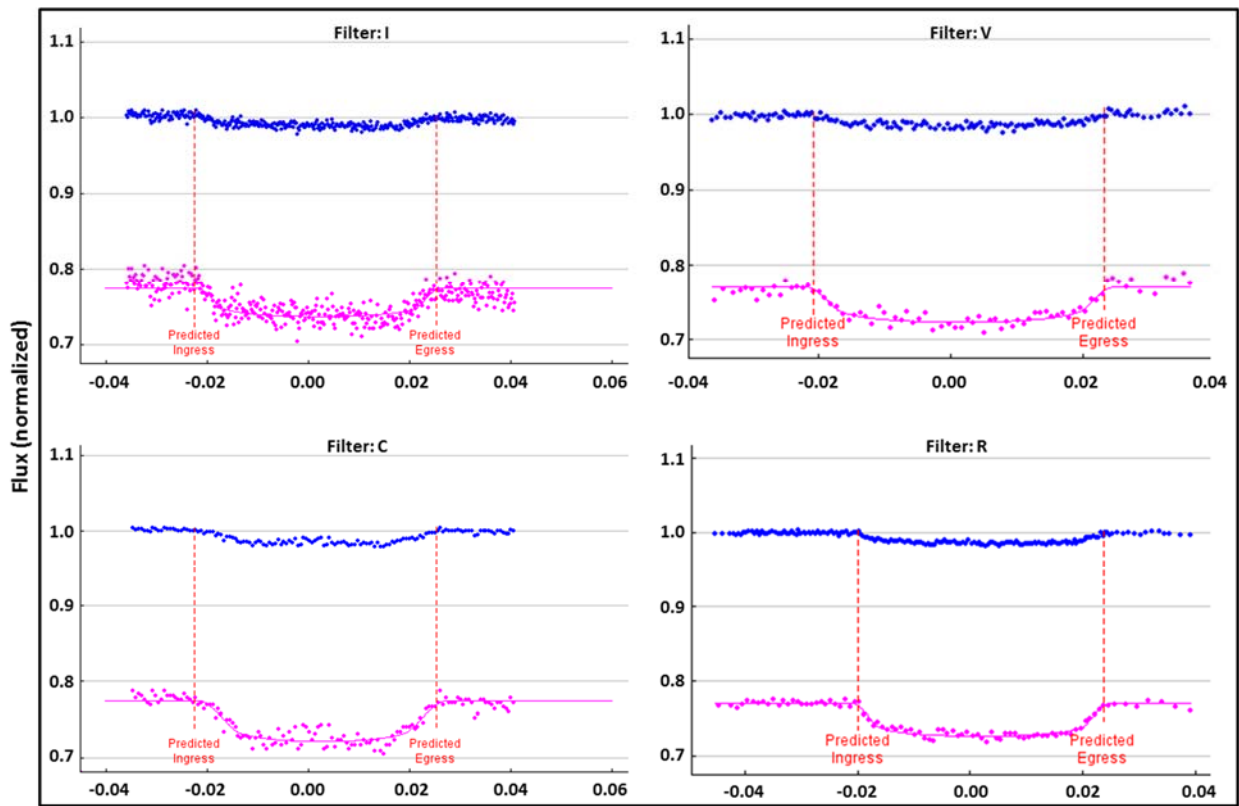
A6. Light curves of Planet HAT-P-30 b

Appendix B.

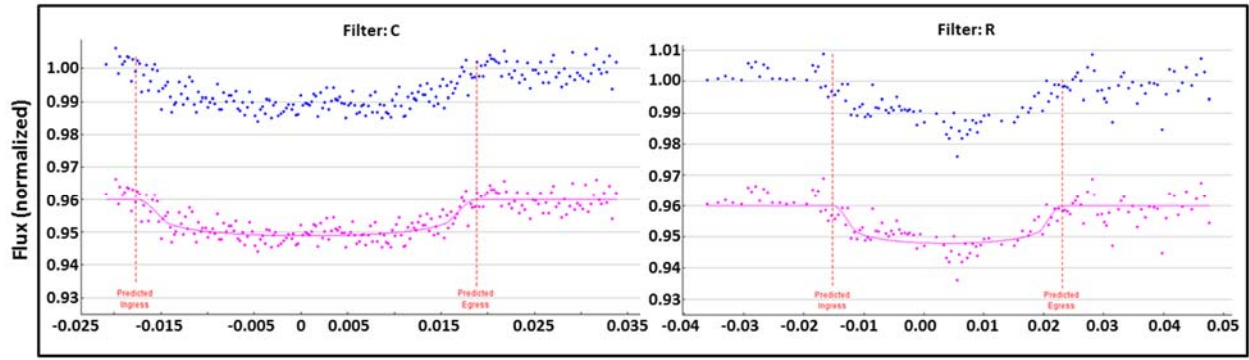
In figures B1-B6, the horizontal axis is plotted based on Phase and the zero point in the graph is equal to T_c (BJD_{TDB}). The vertical axis is based on the flux of the star that is normalized to 1. The raw data are shown as solid blue dots which are plotted with no fit, while the solid magenta dots show the same data assuming that it will reflect a dip in brightness due to the exoplanet's transit, which is shown by the magenta line through the data. The duration of the transit completely lies inside the predicted times of ingress and egress.



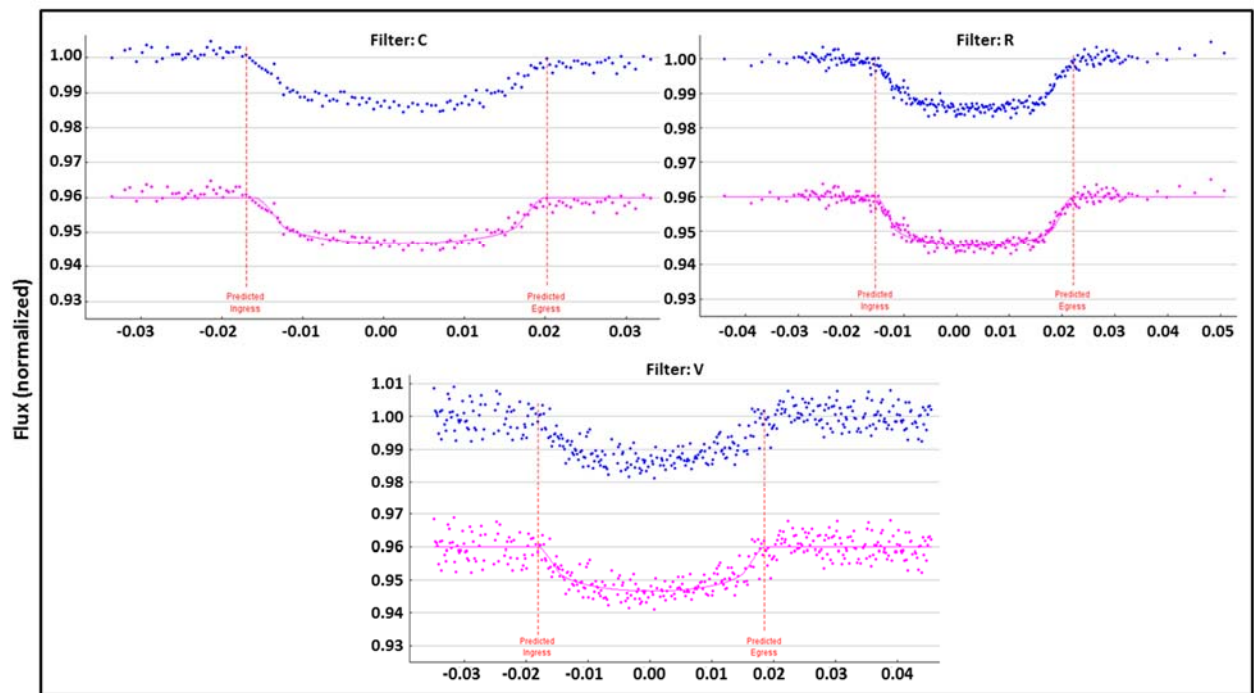
B1. HAT-P-8 b



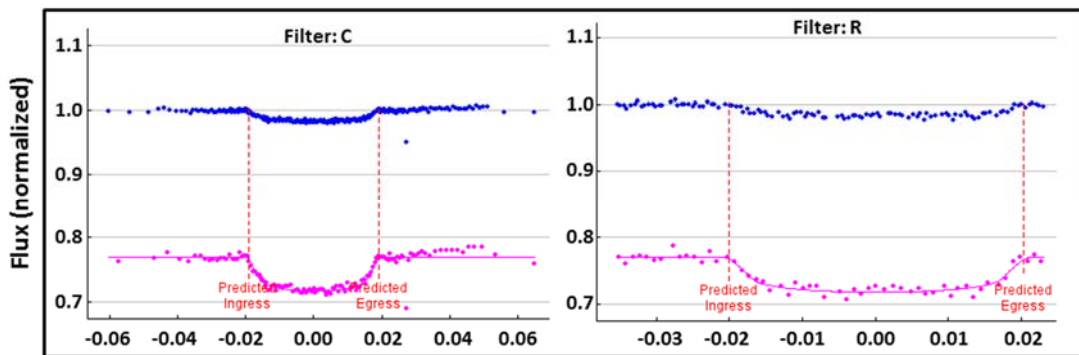
B2. HAT-P-16 b



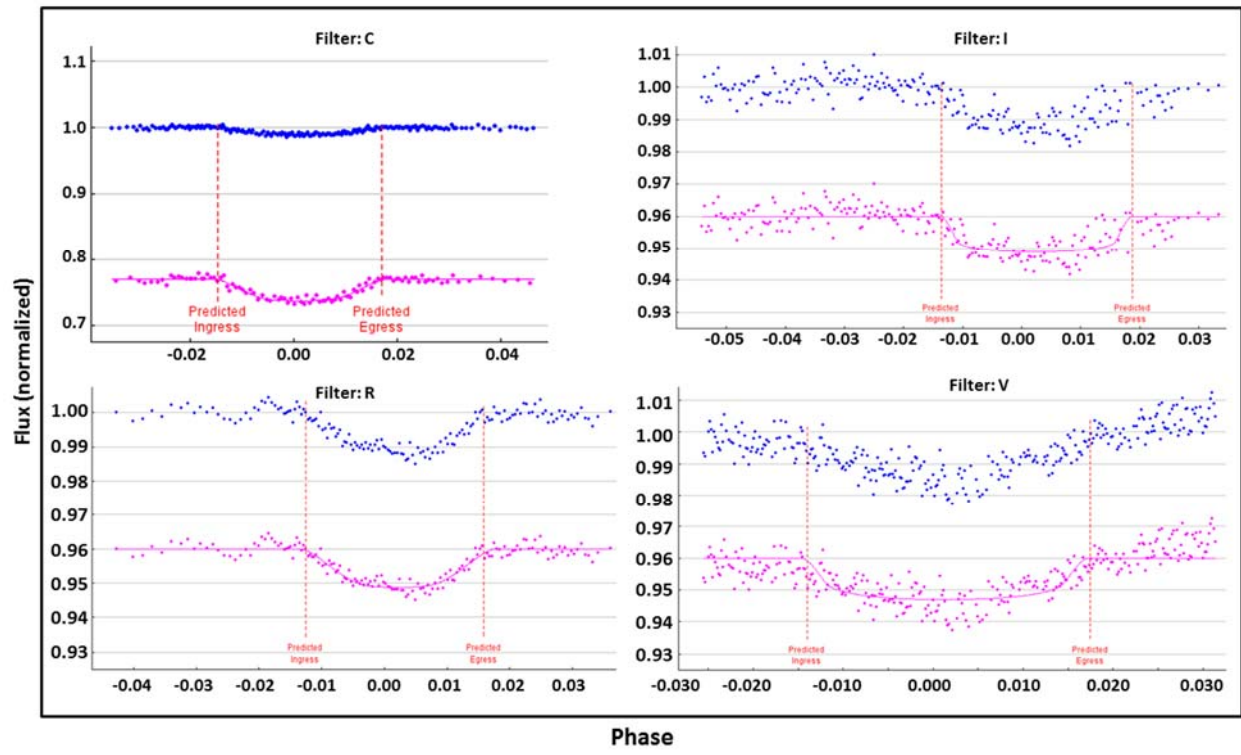
B3. HAT-P-21 b



B4. HAT-P-22 b



B5. HAT-P-28 b



B6. HAT-P-30 b